 CMES, vol.57, no.3, pp.205-224, 2010

Directional Cohesive Elements for the Simulation of Blade Cutting of Thin Shells

A. Frangi[1], **M. Pagani**[1], **U. Perego**[1] **and R. Borsari**[2]

Abstract: This paper is concerned with the finite element simulation of a thin membrane cutting by a sharp blade. Smeared crack finite element approaches appear to be unsuitable for this purpose, since very small elements would be required to conform to the sharp edge of the cutter. Furthermore, when the membrane material is very ductile, classical interface cohesive elements, where the cohesive forces are transmitted in the direction of the crack opening displacement, cannot correctly reproduce situations where the blade crosses the process zone. A simplified approach, based on the new concept of “directional" cohesive elements, is here proposed for a computationally effective simulation of this type of problems. Whenever a crack is opening, cohesive “cable" elements are introduced between the separating nodes. These elements are geometric entities which can be monitored throughout the analysis to detect possible contact with the blade. When this happens, the cables transmit in a straightforward way cohesive forces to the crack flanks in different directions. The procedure has been tested against a real cutting process providing encouraging results with relatively coarse meshes. The calibration of the material properties of the cohesive cables is also briefly discussed.

Keywords: blade cutting, cohesive crack, finite elements, shells

1 Introduction

The numerical simulation of fracture and fragmentation of shells and plates is a timely topic in computational structural engineering and is receiving increasing attention. Since many years, most explicit commercial finite element codes (see e.g. Abaqus and LS-Dyna) offer the possibility to simulate crack propagation in shells by eliminating from the model those finite elements where developing damage has reached a critical threshold. While this provision provides good results for the simulation of diffused damage due to explosions or crashes against large obstacles,

[1] Dept. Structural Engineering, Politecnico di Milano, P.za L. da Vinci 32, 20133 Milan, Italy.
[2] Tetra Pak Packaging Solutions, via Delfini 1, 41100 Modena, Italy

it is not convenient for the simulation of the propagation of isolated cracks in large structures or of localized damages produced by sharp obstacles. These type of problems appear to be better tackled by approaches based on the use of cohesive fracture models, capable to transmit cohesive forces across either an intra-element or inter-element displacement discontinuity.

As noted in [Song and Belytschko (2009)], the literature on cohesive crack propagation in shells is rather limited. Potyondy, Wawrzynek, and Ingraffea (1995) used standard shell finite elements with stress intensity factor calculations and remeshing at different scales to simulate crack propagation in pressurized fuselage structures. Li and Siegmund (2002), developed a cohesive interface element for the simulation of crack growth in thin metal sheet to be used in shell element meshes of the finite element code Abaqus. Cirak, Ortiz, and Pandolfi (2005) proposed an inter-element cohesive crack model based on Kirchhoff shell theory. Areias and Belytschko (2005) and Areias, Song, and Belytschko (2006) formulated a Mindlin-Reissner and a Kirchhoff type shell element, respectively, for fracture analysis based on the Extended Finite Element Method (XFEM). Zavattieri (2006) proposed an interface cohesive element to be placed between four node Belytschko-Lin-Tsay [Belytschko, Lin, and Tsay (1984)] shell elements, whereby the damage contribution due to the bending moment transmitted across the interface is explicitly taken into account. More recently, Song and Belytschko (2009) developed an XFEM shell element, also based on Belytschko-Lin-Tsay element, endowed with a nonlocal strain-based fracture criterion. The method was applied to the simulation of crack propagation in metallic pipes.

The mechanics of cutting a shell with a sharp object or tool has attracted particular attention in the field of naval engineering for the development of ship grounding models. Analyzing the kinematics of the deformation of a metal sheet initially cut by a sharp wedge, Wierzbicki and Thomas (1993) identified three separate dissipation mechanisms: “far-field”plastic deformation (global mechanism); “near-tip”fracture (local mechanism) and friction. They also developed a simplified analytical model for the approximate quantification of the contribution of each mechanism to the total work. For the same type of problem, Zheng and Wierzbicki (1996) developed a simplified model capable to predict the cutting force needed for the steady-state wedge cutting of a metal sheet. Muscat-Fenech and Atkins (1998) studied experimentally the collision of plates against either blunt or sharp obstacles, with relative motion having both normal and parallel components to the plate. The aim was the determination of horizontal and vertical forces experienced by the plate for the different tested collision conditions. More recently, Simonsen and Törnqvist (2004) carried out a combined experimental-numerical investigation for the calibration of crack propagation criteria in large shell structures. The proposed

criteria were then validated by simulating by LS-Dyna a large scale grounding experiment where a double bottom shell structure was grounded and torn on a conical obstacle.

A molecular numerical model for the simulation of cutting has been recently proposed by Lin and Ye (2009) at the nanoscale where an assemblage of copper atoms is cut by diamond blades with different shapes.

An accurate numerical tool for the simulation of blade cutting would result extremely useful also in biomedical (especially surgical) applications. Chanthasopeephan, Desai, and Lau (2007), conducted experimental tests and finite element simulations on the scalpel cutting of a pig liver. When open or laparoscopic surgery involves the cutting of thin sheets, the most effective tools are scissors. Mahvash, Voo, Kim, Jeung, Wainer, and Okamura (2008) developed an analytical model to calculate forces applied to scissors during cutting of tissues. The mechanics of scissors cutting has also been studied extensively by Atkins and coworkers [Atkins, Xu, and Jeronimidis (2004); Atkins and Xu (2005); Atkins (2006)], providing models for the determination of the cutting forces and the definition of the optimal blade shape.

It is also worth mentioning the recently published treatise [Atkins (2009)] which presents a comprehensive account of the state of the art of the research on cutting engineering.

The present work is concerned with the development of a finite element model for the simulation of the blade cutting of thin membranes of the type used in the carton packaging industry to seal a package containing liquid food. The membrane is typically a layered composite, with a total thickness ranging from 70 to 85 μm, made of a thin aluminium layer (6-9 μm) and various low-density polyethylene (LDPE) coating layers. In most cases, the composite is laminated by extruding the LDPE powder directly onto the aluminium layer. A typical response of a uniaxial test of one of these materials is shown in Fig. 1, from which the main features can be noticed:

- the two curves refer to tests on samples extracted in the lamination machine direction (MD) and cross-machine (CD) direction, and only a mild anisotropy can be observed;
- the nominal stress reaches a peak followed by a sudden drop coinciding with the rupture of the aluminium layer;
- the failure of the aluminium layer is followed by a long plateau, usually corresponding to the occurrence of localized necking deformation, where the molecules of the LDPE realign along the direction of loading;

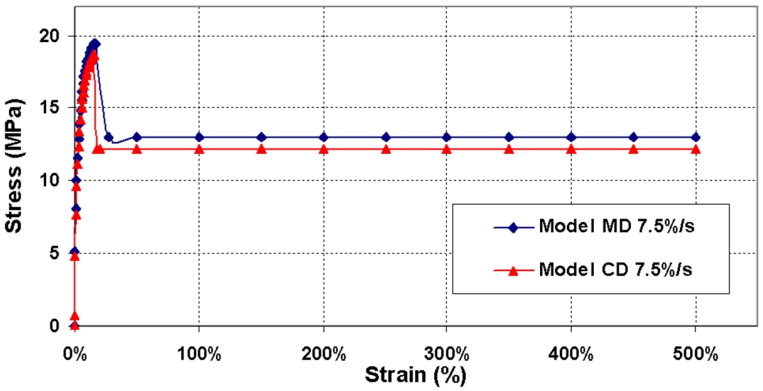

Figure 1: Typical uniaxial response of layered composite for food packaging.

- the limit nominal strain of 500% corresponds to the cross-head limit of the testing rig and not to the failure of the specimen, which has a typical failure nominal strain of 700-900%.

The objective of the opening process is to create a circular hole of a diameter of approximately 15 mm, in a region of the package where a hole has been pre-laminated in the paperboard (Fig. 2a) to reduce the force necessary to cut the laminate. In the hole region there is no paper and only thin aluminium and polymeric layers have to be cut. The hole is produced using the applied cap shown in Fig. 2b. Thanks to a screw thread, the cap rotation transmits the motion to the high-density polyethylene (HDPE) blades of the type shown in Fig. 2c. The opening tool consists of several teeth (four in the figure) which undergo a motion with both normal and tangential components to the laminate surface.

As it will be discussed in the following sections, the standard cohesive interface elements are not suited for the simulation of this type of cutting, dominated by the sharpness of the tooth blade and by the extremely high failure opening of the cohesive interface. The objective of this work is then to develop a new concept of “directional" cohesive element, to be placed at the interface between adjacent shell elements, where the cohesive forces can have different directions on the two sides of the crack whenever the cohesive region is crossed by the cutting blade.

The new cohesive element has been implemented in a shell finite element code and the simulation tool has been validated against the results of an opening test.

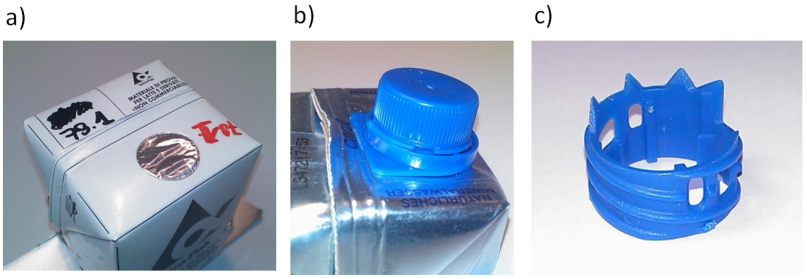

Figure 2: Example configuration of opening system:a) package with pre-laminated hole (PLH); b) applied cap; c) cutting HDPE teeth.

2 Kinematic description

Consider a constant thickness shell body whose geometry is parametrized in terms of the convective coordinates ξ^1, ξ^2, ξ^3

$$\mathbf{X} = \Phi(\xi^1, \xi^2, \xi^3) = \bar{\Phi}(\xi^1, \xi^2) + \xi^3 \mathbf{T}(\xi^1, \xi^2) \qquad -\frac{h}{2} \leq \xi^3 \leq \frac{h}{2} \tag{1}$$

where $\mathbf{X}$ is the position vector of a material point in the shell body; $\bar{\mathbf{X}} = \bar{\Phi}(\xi^1, \xi^2)$ is the position vector of points belonging to the shell middle surface $\mathscr{M}$ ($\xi^3 = 0$), with boundary $\partial\mathscr{M}$; the unit vector $\mathbf{T}(\xi^1, \xi^2)$ denotes the director field and h is the shell thickness. According to the Mindlin-Reissner theory, $\mathbf{T}$ is assumed to be normal to the middle surface in the original configuration but is not forced to remain so during the deformation.

At time $t \in [0, T]$, the shell configuration is defined by the mapping $\mathbf{x} = \chi_t(\mathbf{X})$ and is parametrized as

$$\mathbf{x} = \varphi(\xi^1, \xi^2, \xi^3) = \bar{\varphi}(\xi^1, \xi^2) + \xi^3 \mathbf{t}(\xi^1, \xi^2) \qquad -\frac{h}{2} \leq \xi^3 \leq \frac{h}{2} \tag{2}$$

with obvious meaning of symbols. The deformation (2) accounts for the inextensibility assumption of the director field. The displacement $\mathbf{u}$ at a point $\mathbf{X}(\xi^1, \xi^2, \xi^3)$ is then defined as

$$\mathbf{u}(\xi^1, \xi^2, \xi^3) = \mathbf{x}(\xi^1, \xi^2, \xi^3) - \mathbf{X}(\xi^1, \xi^2, \xi^3) = \bar{\mathbf{u}}(\xi^1, \xi^2) + \xi^3 [\mathbf{t}(\xi^1, \xi^2) - \mathbf{T}(\xi^1, \xi^2)] \tag{3}$$

It is convenient to define the covariant basis vectors $\{\mathbf{A}_i\}$ and $\{\mathbf{a}_i\}$, $i = 1, 2, 3$, on the shell middle surface in the original and deformed configurations, respectively.

The basis vectors belonging to the local tangent plane are defined as $\mathbf{A}_\alpha = \bar{\Phi}_{,\alpha}$ and $\mathbf{a}_\alpha = \bar{\varphi}_{,\alpha}$, $\alpha = 1,2$, while the unit vectors normal to the middle surface are defined as

$$\mathbf{A}_3 = \frac{\mathbf{A}_1 \times \mathbf{A}_2}{\|\mathbf{A}_1 \times \mathbf{A}_2\|}, \quad \mathbf{a}_3 = \frac{\mathbf{a}_1 \times \mathbf{a}_2}{\|\mathbf{a}_1 \times \mathbf{a}_2\|} \tag{4}$$

The Green-Lagrange strain tensor is expressed in the shell body as

$$\mathbf{E} = \frac{1}{2}(\mathbf{g}_i \cdot \mathbf{g}_j - \mathbf{G}_i \cdot \mathbf{G}_j)\mathbf{G}^i \otimes \mathbf{G}^j = E_{ij}\mathbf{G}^i \otimes \mathbf{G}^j \tag{5}$$

where $\mathbf{G}_i$ and $\mathbf{G}^i$ are the covariant and contravariant base vectors, respectively, in the reference configuration and $\mathbf{g}_i$ is the covariant basis in the current configuration. These are defined as

$$\mathbf{G}_\alpha = \Phi_{,\alpha} = \mathbf{A}_\alpha + \xi^3 \mathbf{T}_{,\alpha} \tag{6}$$

$$\mathbf{G}_3 = \Phi_{,3} = \mathbf{T} = \mathbf{A}_3 \tag{7}$$

$$\mathbf{g}_\alpha = \varphi_{,\alpha} = \mathbf{a}_\alpha + \xi^3 \mathbf{t}_{,\alpha} \tag{8}$$

$$\mathbf{g}_3 = \varphi_{,3} = \mathbf{t} \tag{9}$$

Let us consider now a through-crack developing in the shell body. In the initial reference system, the image of the crack surface is denoted as $\Gamma_c \times [-\frac{h}{2}, \frac{h}{2}]$, where Γ_c is its intersection with the middle surface. In the current configuration the crack is open and its flanks $\Gamma_c^+ \times [-\frac{h}{2}, \frac{h}{2}]$ and $\Gamma_c^- \times [-\frac{h}{2}, \frac{h}{2}]$ are separated.

The displacement jump across the crack is obtained from (3) as

$$\mathbf{w} = [\![\mathbf{u}]\!] = \mathbf{u}^+ - \mathbf{u}^- = \bar{\mathbf{w}} + \xi^3 [\![\mathbf{t}]\!] \tag{10}$$

Points belonging to the crack surface $\Gamma_c \times [-\frac{h}{2}, \frac{h}{2}]$ in the initial configuration are defined by the mapping

$$\mathbf{X}_c = \bar{\Phi}_c(\xi^1(\eta), \xi^2(\eta)) + \xi^3 \mathbf{T}_c(\xi^1(\eta), \xi^2(\eta)) \tag{11}$$

where $\bar{\Phi}_c(\eta)$ is the parametric representation of Γ_c on the middle surface and η is a scalar parameter.

Defining as

$$\mathbf{A}_c = \frac{\partial \xi^\alpha}{\partial \eta} \bar{\Phi}_{c,\alpha} \quad \mathbf{A}^n = \frac{\mathbf{A}_c \times \mathbf{T}_c}{\|\mathbf{A}_c \times \mathbf{T}_c\|} = \mathbf{A}_n \tag{12}$$

the tangent and normal vectors to Γ_c on the middle surface, a covariant basis for the crack surface in the original configuration can be defined as

$$\mathbf{G}_c = \frac{\partial \xi^\alpha}{\partial \eta}(\bar{\Phi}_{c,\alpha} + \xi^3 \mathbf{T}_{c,\alpha}) = \mathbf{A}_c + \xi^3 \frac{\partial \xi^\alpha}{\partial \eta}\mathbf{T}_{c,\alpha} \tag{13}$$

$$\mathbf{G}_3 = \mathbf{T}(\xi^1(\eta), \xi^2(\eta)) = \mathbf{T}_c \tag{14}$$

$$\mathbf{G}^n = \frac{\mathbf{G}_c \times \mathbf{G}_3}{\|\mathbf{G}_c \times \mathbf{G}_3\|} = \mathbf{G}_n \tag{15}$$

3 Weak form of equilibrium

Let $\mathbf{p}dS$ be the cohesive force acting on an elementary area $dS = \|\mathbf{G}_c \times \mathbf{G}_3\| d\xi^3 d\eta$ of the crack reference surface $\Gamma_c \times [-\frac{h}{2}, \frac{h}{2}]$. Equilibrium is enforced in weak form through the virtual work equality

$$\delta\Pi_{\text{int}} - \delta\Pi_{\text{ext}} = 0 \tag{16}$$

where

$$\delta\Pi_{\text{ext}} = \int_V \mathbf{f} \cdot \mathbf{u} dV + \int_{\partial V} \bar{\mathbf{p}} \cdot \mathbf{u} dS \tag{17}$$

$$\delta\Pi_{\text{int}} = \delta\Pi_{\text{int},V} + \delta\Pi_{\text{int},c} = \tag{18}$$

$$= \int_{\mathscr{M}\setminus\Gamma_c} \int_{-\frac{h}{2}}^{\frac{h}{2}} \mathbf{S} : \delta\mathbf{E} \mu d\xi^3 d\mathscr{M} + \int_{\Gamma_c} \int_{-\frac{h}{2}}^{\frac{h}{2}} (\mathbf{p}^- \cdot \delta\mathbf{u}^- + \mathbf{p}^+ \cdot \delta\mathbf{u}^+) \gamma d\xi^3 d\Gamma_c \tag{19}$$

In equations (17) and (19), V is the volume occupied by the shell body in the reference configuration, ∂V is the portion of the boundary where traction boundary conditions are prescribed, $\mathbf{f}$ and $\bar{\mathbf{p}}$ denote the assigned body and traction forces, respectively, $d\mathscr{M} = \|\mathbf{A}_1 \times \mathbf{A}_2\| d\xi^1 d\xi^2$ is the middle surface infinitesimal element, $\mathbf{S}$ is the second Piola-Kirchhoff stress tensor, μ and γ are defined as

$$\mu = \frac{\|\mathbf{G}_1 \times \mathbf{G}_2\|}{\|\mathbf{A}_1 \times \mathbf{A}_2\|}, \quad \gamma = \frac{\|\mathbf{G}_c \times \mathbf{G}_3\|}{\sqrt{\mathbf{A}_c \cdot \mathbf{A}_c}} \tag{20}$$

and account for the curvature of the middle surface and of Γ_c, respectively, while $\delta\mathbf{E}$, $\delta\mathbf{u}^-$ and $\delta\mathbf{u}^+$ are the variations of the kinematic fields, conjugate to $\mathbf{S}$ and $\mathbf{p}^-$, $\mathbf{p}^+$.

In classical cohesive formulations, equilibrium conditions at the interface require that $\mathbf{p}^+ = -\mathbf{p}^- = \mathbf{p}$ and the internal work on the cohesive interface is rewritten as

$$\delta\Pi_{\text{int},c} = \int_{\Gamma_c} \int_{-\frac{h}{2}}^{\frac{h}{2}} \mathbf{p} \cdot \delta\mathbf{w}\gamma d\xi^3 d\Gamma_c \tag{21}$$

4 The concept of directional cohesive element

Standard finite element approaches to fracture, based on the introduction of a cohesive interface between adjacent shell elements, usually follow these steps: the deformation and the state of stress in the uncracked shell structure is determined; wherever a prescribed propagation criterion is exceeded at a node, that node is duplicated and a displacement discontinuity is allowed along the element interfaces, in the direction defined by the propagation criterion; opposite cohesive forces are introduced across the discontinuity. The direction of the opposite forces depends only on the direction of the displacement jump and on the adopted cohesive law. When the material is quasi-brittle and/or the impacting object is blunt, there is no interference between the object and the cohesive region because the ultimate cohesive opening displacement is much smaller than the typical size of the object. On the contrary, when the material is very ductile, as in the case of the laminate considered in Fig. 1, or the cutting blade is sharp, it may well happen that the blade intersects the trajectory of the cohesive forces, giving rise to inaccurate predictions of the crack propagation. This problem does not occur when crack propagation is simulated by removing damaged elements from the mesh, as it is currently done in advanced commercial finite element codes. In this case the contact algorithm is active on the element until the element is removed and penetration of the blade is not allowed. However, this approach requires a mesh of the shell body fine enough to conform to the blade edge. If the blade is sharp, as in the case of the cutters of interest herein, an accurate description of the propagation can lead to prohibitive computational costs.

A different approach is adopted in this work, based on the following specific features of the fracture nucleation and propagation in the considered aluminium-polymeric composite.

- The aluminium layer is quasi-brittle, especially if compared to the highly ductile LDPE layers.
- After the aluminium layer has failed, in correspondence to the sudden drop in Fig. 1, the load is transmitted entirely by the highly ductile polymeric layers along the constant stress plateau of Fig. 1.

- In the plateau region of Fig. 1, plastic strains localize in a very narrow band, where the aluminium layer is broken, mainly located in the region in contact with the cutter edge, while the material outside the process zone unloads in the elastic regime. In fact, the sharper is the blade, the more localized is the damage produced in the laminate. In a sheet of paper cut by a razor blade, the sheet remains elastic and the cut pieces match almost perfectly to each other [Atkins, Xu, and Jeronimidis (2004)]. This observation allows one to interpret the inelastic part of the stress-strain behavior of Fig. 1, as the behavior of the material in the process zone. The cohesive law is then assumed in the form shown in Fig. 4, where ℓ is the current length of material fibers in the cohesive zone.

- As noted in [Atkins and Xu (2005)] on the basis of experimental tests, the specific surface work required for crack propagation is unaffected by relative blade motion and does not depend on the mode of fracture, while it is influenced by friction between the blade and the sheet. As a consequence, only Mode I tearing will be considered in the fracture process and perfect adhesion will be postulated between the cutter blade and the polyethylene fibrils in the process zone.

- In view of the small thickness of the shell and of its small bending inertia, the bending strength in the cohesive region can be neglected. The internal work contribution of the cohesive interface in Eq. (19) can be rewritten neglecting in Eq. (3) the displacement variations along the thickness:

$$\delta\Pi_{\text{int},c} = \int_{\Gamma_c}\int_{-\frac{h}{2}}^{\frac{h}{2}} (\mathbf{p}^- \cdot \delta\bar{\mathbf{u}}^- + \mathbf{p}^+ \cdot \delta\bar{\mathbf{u}}^+)\gamma d\xi^3 d\Gamma_c \tag{22}$$

$$= \int_{\Gamma_c} (\mathbf{P}^- \cdot \delta\bar{\mathbf{u}}^- + \mathbf{P}^+ \cdot \delta\bar{\mathbf{u}}^+) d\Gamma_c \tag{23}$$

where it has been defined

$$\mathbf{P} = \int_{-\frac{h}{2}}^{\frac{h}{2}} \mathbf{p}\gamma d\xi^3 \tag{24}$$

The cohesive force is then integrated along the element interfaces using the trapezoidal rule, giving rise in the discretized model to cohesive forces $\mathbf{F}_i^{\pm}$ concentrated at the separated nodes $i^{\pm}$.

Based on these observations and assumptions, the proposed approach can be described as follows. When the selected fracture criterion is met at a given node,

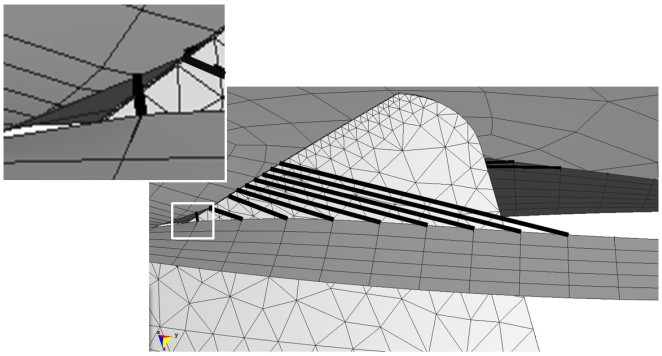

Figure 3: Cohesive forces between detaching elements.

the node is duplicated and it is assumed that cohesive forces $\mathbf{F}_i^{\pm}$ are transmitted between the newly created pair of nodes $i^{\pm}$ by a massles "cable", i.e. a truss element introduced ad hoc in the model in correspondence of each pair of separating nodes. It is worth stressing that, in the current implementation, the cohesive cables are attached to nodes lying in the middle surface of the shell, but different options in which cables are e.g. attached to Gauss points along fractured edges are equally feasible.

In the present contribution, fracture is activated when the maximum principal stress σ_I reaches a given threshold σ_F. The cohesive force exerted by the cable on the two nodes is set, for the very first time step after crack initiation, to $\pm\sigma_F A_i \mathbf{m}$, where A_i is the area of the cohesive surface through the shell pertinent to the node i and $\mathbf{m}$ is a direction which is "orthogonal" in the average to the separating flanks.

During the subsequent time steps the nodes separate and the cable is a straight segment naturally endowed with a length ℓ which is simply the distance between the nodes. The direction of the cohesive force is provided by the opening vector $\bar{\mathbf{w}}$ defined in Eq. (10). The intensity of the force is σA_i, where σ depends on the specific cohesive constitutive law adopted for the cable. In the present case, this has been selected as the non-holonomic law of Figure 4. This is the case of the first cable in the magnified frame on the left in Figure 3, which has not been contacted by the cutter yet.

Unlike in standard cohesive approaches, the cable element is a well defined geometric entity, and its contact against the cutting blade can be checked throughout the analysis duration, even though, in view of the sharpness of the cutter and to enhance the computational efficiency of the procedure, contact is here only checked against points belonging to the cutting edge (and not against the cutting sides).

When a point of a cable element is detected to be in contact with the blade, the cable element is subdivided in two truss elements by introducing a joint in correspondence of the contact point. The length of the cable is now defined as the sum of the lengths of the two constituent trusses. Due to the high level of friction between the cutter and the LPDE membrane, it is assumed that the contact point cannot move along the cutting edge of the cutter. Two forces $\mathbf{F}_i^+$ and $\mathbf{F}_i^-$ of the same magnitude are assumed to be transmitted by the two branches of the cable to the crack flanks. The direction of the forces is however different at the two nodes i^+ and i^-, being determined by the directions of the truss elements connecting the nodes to the contact point (see Fig. 3). The force magnitude in the cable is obtained from the stress in Fig. 4 corresponding to the total cable length ℓ. In this way, the cohesive force can be transmitted between the crack flanks in a direction which is not along the line connecting the separating nodes, correctly taking into account the presence of the cutter. When the current length of the cable exceeds the limit value ℓ_U, the cable is removed and no cohesive forces are applied to the associated nodes.

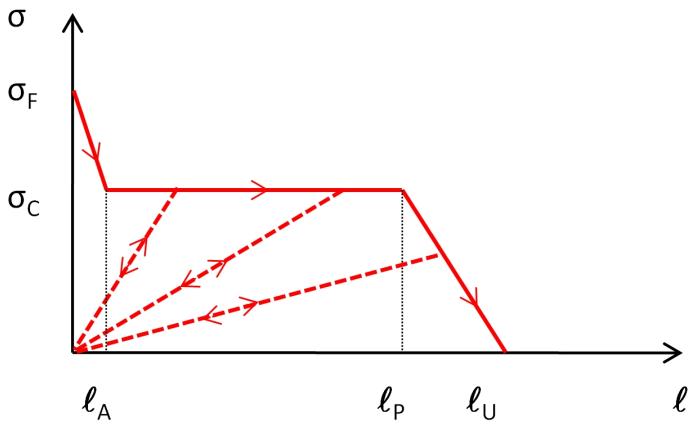

Figure 4: Constitutive modeling of cohesive elements.

5 Example of application

We focus here on the simulation of a specific cutting process where the membrane is a circle of radius $R = 10.2$ mm and thickness $h = 0.074$ mm and is assumed to be clamped on the outer boundary. The aluminium foil is approximately $1/10^{th}$ of the overall thickness.

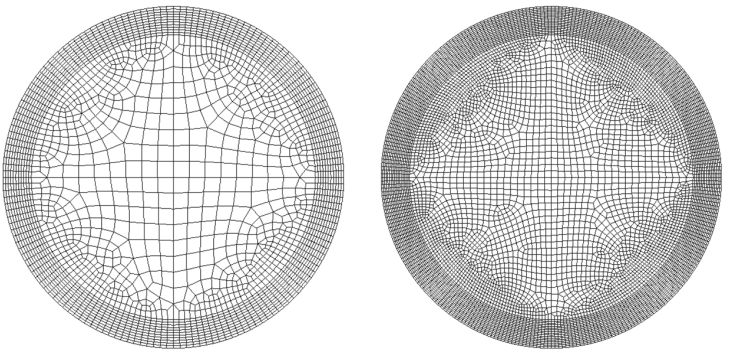

Figure 5: Different meshes M_1 and M_2 employed for the deformable shell.

The cutting tool employed is depicted in Figure 2 and has an average radius of 9.4 mm. The radius of curvature at the cutting edge is approximatively of 0.1 mm. In view of this small size, in the finite element model it is represented as the sharp intersection of two element edges. The tool is treated here as a rigid body undergoing a prescribed rotation and vertical displacement simulating the true opening process.

In order to test possible mesh-dependence of results, the membrane has been discretized with two different meshes of quadrilateral MITC4 elements [Bathe (1996)], as illustrated in Figure 5. The coarse mesh M_1 contains 2634 elements, while the finer mesh M_2 has 8647 elements. For the application of the fracture activation criterion, stresses have been extrapolated at nodes using the superconvergent patch recovery technique proposed by Zienkiewicz and Zhu (1992).

5.1 Choice of constitutive parameters

At the beginning of the analysis, the composite lamina is simulated as an equivalent homogenized and isotropic membrane endowed with a linear constitutive law expressing Piola-Kirchhoff stresses in terms of Green-Lagrange strains with Young modulus $E = 1678$ MPa and Poisson coefficient $\nu = 0.3$.

Cohesive elements are dynamically activated only when the fracture criterion described in Section 4 is met. Fracture parameters for the cohesive elements have been selected as $\sigma_F = 18$ MPa; $\sigma_C = 12$ MPa, $\ell_A = 0.5$ mm, $\ell_P = 3$ mm and $\ell_U = 4$ mm. It is worth stressing that cohesive elements can only be activated along the edges of the shell mesh, thus excluding a priori any form of remeshing during the analysis.

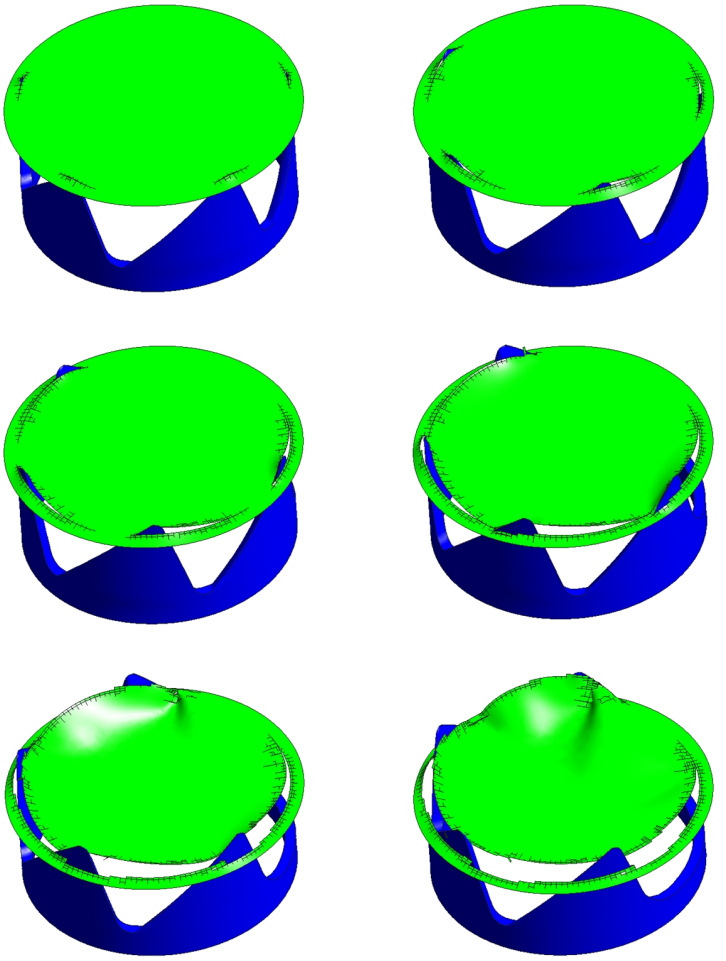

Figure 6: Evolution of the opening process simulated with mesh M_1.

While the choice of σ_F and σ_C has been performed by simple inspection of Figure 1, the selection of ℓ_A, ℓ_P and ℓ_U is more delicate and deserves some comments. As far as the aluminium layer is concerned, Pardoen, Marchal, and Delannay (2002) report a limit toughness of $G_f = 30\,\text{kJ/m}^2$ for aluminium plates of vanishing thickness (toughness in the plane-stress limit). On the other hand, Kao-Walter (2004) reports on significantly smaller values coming from experimental tests on thin free-standing aluminium foils (6-7 μm). However, Kao-Walter also notes that unexpectedly higher values of fracture energy are obtained for LDPE-aluminium laminates, hinting that the presence of the other layers constrains the development of through-thickness plastic strains in the aluminium foil, increasing in this way its fracture energy. For these reasons, and in the absence of further experimental data, a fracture energy $G_f = 30\,\text{kJ/m}^2$ is adopted. In order to estimate the dissipation associated to LDPE fracture, following Section 4, the concept of essential work of fracture [Williams and Rink (2007)] is employed, adopting $W_f = 45\,\text{kJ/m}^2$, which is in agreement with the average values obtained from laboratory experiments on free-standing LDPE foils (see also e.g. [Pegoretti, Castellani, Franchini, Mariani, and Penati (2009)]). The average of the dissipation energies, weighted through the thickness of the different layers, gives an overall dissipation per unit thickness of $43.5\,\text{kJ/m}^2$, which corresponds to the area beneath the curve in Figure 4: $(1/2)(\sigma_F - \sigma_C)\ell_A + (1/2)\sigma_C(\ell_P + \ell_U)$. The choice of the values of ℓ_A, ℓ_P and ℓ_U indicated above avoids steep softening branches which might induce numerical oscillations. Different choices are not expected to affect results considerably, as long as the dissipation energy is preserved.

5.2 Numerical analysis

Due to the strong geometrical and material non-linearities involved in the problem at hand, the equations of motions are integrated in time by making recourse to the central difference explicit algorithm. At each time step, the increment of the director is computed at every node by expressing the angular velocity in a local frame tangent to the shells, thus eliminating any drilling DoF.

The mass matrix is diagonalized, according to the spirit of explicit approaches. However, since in such thin shells the true dynamics of the directors is of no practical interest, a selective scaling for the rotational inertia is applied as explained in [Hughes (1987), chap. 9], in order to increase the maximum allowable time step.

The time steps employed in the simulations with the two meshes M_1 and M_2 are of the order of $\Delta t_1 = 1 \times 10^{-7}$ s and $\Delta t_2 = 0.7 \times 10^{-7}$ s, respectively.

Contact conditions between the rigid cutting tool and the deformable shell are enforced by means of a penalty approach. The cutter is selected as the master surface and a global-local search technique is implemented in order to efficiently monitor

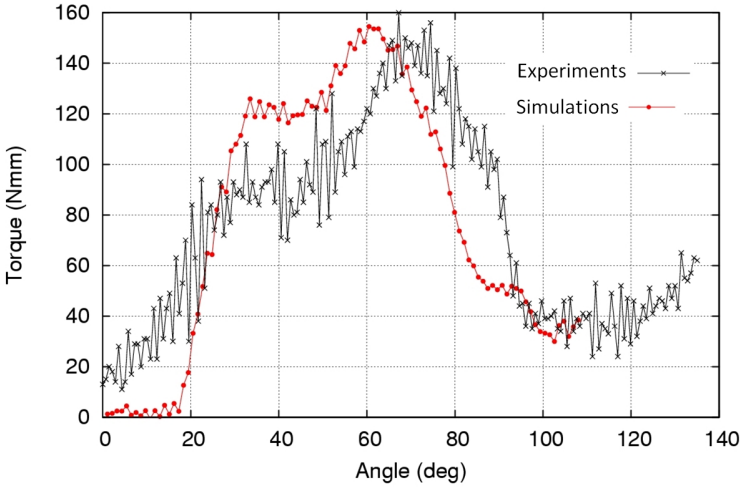

Figure 7: Torque-angle of rotation graph for mesh M_1. Experiments (crosses) vs. numerical results (dots)

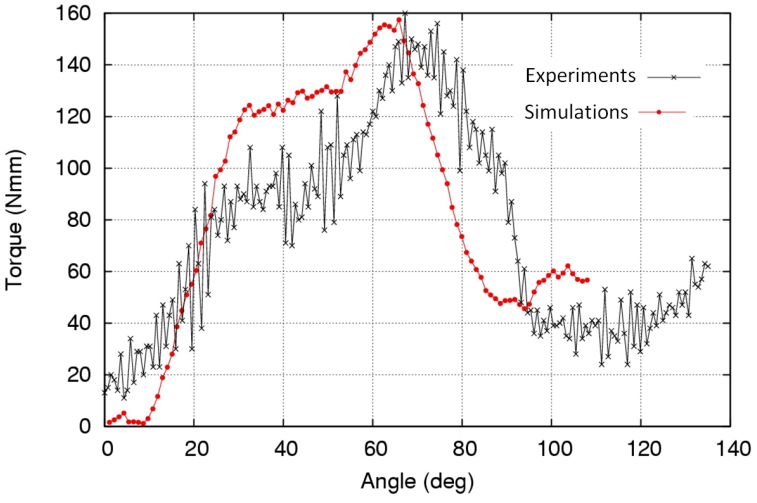

Figure 8: Torque-angle of rotation graph for mesh M_2. Experiments (crosses) vs. numerical results (dots)

the nodes of the shell which are closest to the cutter. When an interpenetration occurs at a point of the cutter of outward normal $\mathbf{n}$, the force $-\lambda f(g)A\mathbf{n}$ is applied to the translational DoF of the node, where $\lambda = 10^4$ N/(mm^3) is the penalty coefficient, A is the shell area associated to the slave node ($1/4$ of the average of the areas of the elements sharing the node itself), g is the absolute value of the interpenetration and f is a smoothing function with:

$$f(g) = \begin{cases} (g/g_M)^3(3g_M - 2g), & \text{if} \quad g < g_M \\ g, & \text{if} \quad g \geq g_M \end{cases}$$

where $g_M = (1/4)h$.

A dissipative term has also been added to the discretized equations. The dissipation matrix is expressed as a weighted sum of the mass and stiffness matrices, with coefficients $\alpha = 0.1$ and $\beta = 5.0\,10^{-8}$ respectively (measured in a unit system consistent with s,mm and N).

All these ingredients have been programmed in a Fortran90 parallel code for shared memory architectures. A typical graphical output is presented in Fig, 6 which collects a series of snapshots of the numerical analysis at different stages of the opening process.

5.3 Experimental validation

An experimental campaign has been conducted in parallel in order to evaluate both the torque as a function of rotation angle of the cutter and to provide videos of the deformation and cracking pattern of the thin membrane.

The comparison between the numerical prediction and experiments in terms of torque vs. rotation angle is presented in Figures 7 and 8 where a very good agreement is observed. The numerical torque is evaluated on the basis of the contact forces between the cutter and the shell.

This results corroborates the basic assumption that an elastic constitutive behaviour for the bulk material should be accurate enough for the evaluation of macroscopic quantities like the opening torque. It is also worth stressing that almost no mesh dependence is observed, in agreement with the common understanding that the simulation of damage and fracture by means of discrete cracking and cohesive elements allows to eliminate the issue of mesh dependence observed in diffused/smeared cracking approaches.

A visual comparison is also attempted in Figure 9 between the snapshots of the simulation and of the experimental video. A good qualitative agreement is observed in terms of fracture pattern and advancement, though the real membrane displays a somehow higher toughness (lower brittleness), possibly associated to a slightly

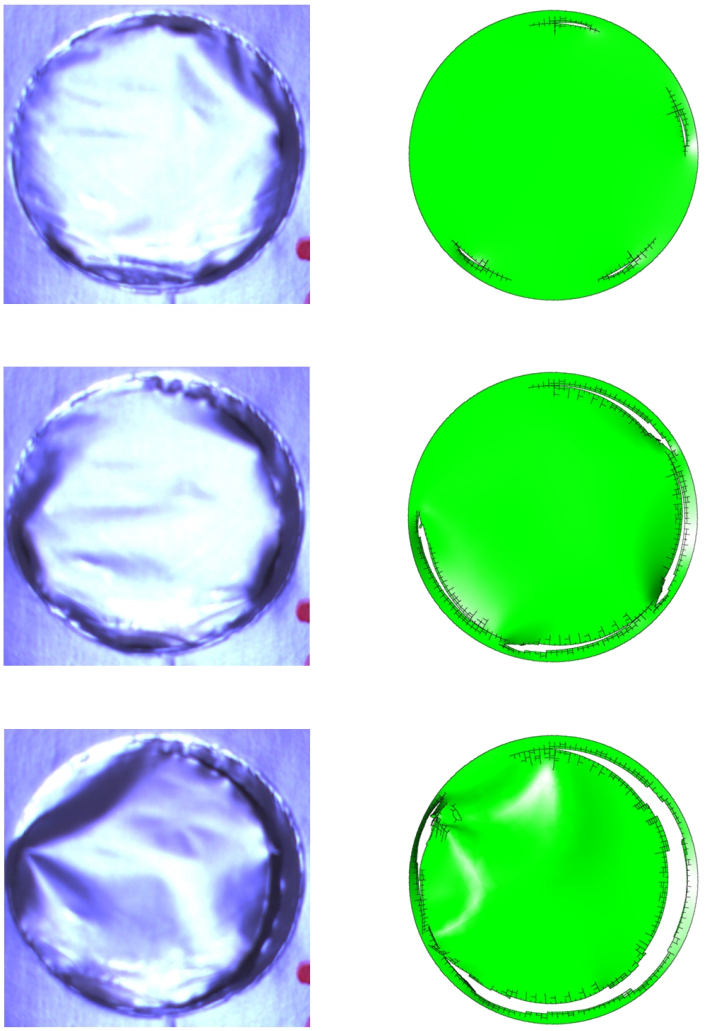

Figure 9: Comparison of fracture advancement and pattern in experiments (left) and simulations (right).

greater bluntness of the real cutter edge with respect to the numerical model, where the blade edge results from the intersection of flat elements and is therefore extremely sharp.

6 Conclusions

We have developed a simplified procedure, based on the definition of "directional" cohesive elements, for the simulation of the blade cutting of thin membranes used in the carton packaging industry to seal packages containing liquid food. The membrane consists of a composite lamina made of thin layers of aluminium and low density polyethylene (LPDE). Since LPDE is a highly ductile material, the post-aluminium-fracture behaviour is crucial to reproduce the macroscopic response of the membrane as measured, e.g., by the torque-rotation angle graph. In standard interface cohesive elements, the direction of the cohesive forces simply depends on the crack opening and cannot account for the presence of sharp cutting tools progressing between the cohesive flanks. A new kind of "directional" cohesive elements has then been introduced which simulate the contact between LPDE and the cutting tool within the fracture process zone and are able to capture the essential phenomena of the opening process. The constitutive law of the cohesive elements has been calibrated on the basis of ad hoc laboratory experiments and of data available in the literature. A validation of the model has been performed against laboratory opening tests and a good agreement has been found with relatively coarse meshes. As expected, the adoption of a cohesive model has eliminated almost completely the dependence of results on the refinement of the mesh which is a major issue in standard FEM simulation since LPDE displays a softening behaviour. One limitation of the present implementation is the absence of plasticity in the shell model for the composite membrane. The introduction of plastic deformations, currently in progress, together with specifically conceived experimental tests for material parameters calibration, should allow to improve the accuracy of the simulation both in quantitative and qualitative terms.

Acknowledgement: The financial support by Tetra Pak Packaging Solutions is kindly acknoweledged.

References

Areias, P. M. A.; Belytschko, T. (2005): Non-linear analysis of shells with arbitrary evolving cracks using xfem. *International Journal for Numerical Methods in Engineering*, vol. 62, no. 3, pp. 384–415.

Areias, P. M. A.; Song, J. H.; Belytschko, T. (2006): Analysis of fracture in thin shells by overlapping paired elements. *Computer Methods in Applied Mechanics and Engineering*, vol. 195, no. 41-43, pp. 5343–5360.

Atkins, A.; Xu, X. (2005): Slicing of soft flexible solids with industrial applications. *International Journal of Mechanical Sciences*, vol. 47, no. 4-5, pp. 479–492.

Atkins, A. G.; Xu, X.; Jeronimidis, G. (2004): Cutting, by 'pressing and slicing,' of thin floppy slices of materials illustrated by experiments on cheddar cheese and salami. *Journal of Materials Science*, vol. 39, no. 8, pp. 2761–2766.

Atkins, T. (2006): Optimum blade configurations for the cutting of soft solids. *Engineering Fracture Mechanics*, vol. 73, no. 16, pp. 2523–2531.

Atkins, T. (2009): *The science and engineering of cutting*. Buttherworth Heinemann, Oxford, UK.

Bathe, K. (1996): *Finite element procedures*. Prentice-Hall Int., Englewood Cliffs, NJ, USA.

Belytschko, T.; Lin, J. I.; Tsay, C. S. (1984): Explicit algorithms for the nonlinear dynamics of shells. *Computer Methods in Applied Mechanics and Engineering*, vol. 42, no. 2, pp. 225–251.

Chanthasopeephan, T.; Desai, J. P.; Lau, A. C. W. (2007): Modeling soft-tissue deformation prior to cutting for surgical simulation: Finite element analysis and study of cutting parameters. *Biomedical Engineering, IEEE Transactions on*, vol. 54, no. 3, pp. 349–359.

Cirak, F.; Ortiz, M.; Pandolfi, A. (2005): A cohesive approach to thin-shell fracture and fragmentation. *Computer Methods in Applied Mechanics and Engineering*, vol. 194, no. 21-24, pp. 2604–2618.

Hughes, T. (1987): *The Finite Element Method: linear static and dynamic finite element analysis*. Prentice-Hall Int., Englewood Cliffs, NJ, USA.

Kao-Walter, S. (2004): *On the Fracture of Thin Laminates*. PhD thesis, Blekinge Institute of Technology, Karlskrona, Sweden, 2004.

Li, W.; Siegmund, T. (2002): An analysis of crack growth in thin-sheet metal via a cohesive zone model. *Engineering Fracture Mechanics*, vol. 69, no. 18, pp. 2073–2093.

Lin, Z.-C.; Ye, J.-R. (2009): Quasi-steady molecular statics model for simulation of nanoscale cutting with different diamond cutters. *CMES: Computer Modeling in Engineering & Science*, vol. 50, no. 3, pp. 227–252.

Mahvash, M.; Voo, L. M.; Kim, D.; Jeung, K.; Wainer, J.; Okamura, A. M. (2008): Modeling the forces of cutting with scissors. *Biomedical Engineering, IEEE Transactions on*, vol. 55, no. 3, pp. 848–856.

Muscat-Fenech, C.; Atkins, A. G. (1998): Denting and fracture of sheet steel by blunt and sharp obstacles in glancing collisions. *International Journal of Impact Engineering*, vol. 21, no. 7, pp. 499–519.

Pardoen, T.; Marchal, Y.; Delannay, F. (2002): Essential work of fracture compared to fracture mechanics-towards a thickness independent plane stress toughness. *Engineering Fracture Mechanics*, vol. 69, no. 5, pp. 617–631.

Pegoretti, A.; Castellani, L.; Franchini, L.; Mariani, P.; Penati, A. (2009): On the essential work of fracture of linear low-density-polyethylene. i. precision of the testing method. *Engineering Fracture Mechanics*.

Potyondy, D. O.; Wawrzynek, P. A.; Ingraffea, A. R. (1995): Discrete crack growth analysis methodology for through cracks in pressurized fuselage structures. *International Journal for Numerical Methods in Engineering*, vol. 38, no. 10, pp. 1611–1633.

Simonsen, B.; Törnqvist, R. (2004): Experimental and numerical modelling of ductile crack propagation in large-scale shell structures. *Marine Structures*, vol. 17, no. 1, pp. 1–27.

Song, J. H.; Belytschko, T. (2009): Dynamic fracture of shells subjected to impulsive loads. *Journal of Applied Mechanics*, vol. 76, no. 5, pp. 051301_1–051301_9.

Wierzbicki, T.; Thomas, P. (1993): Closed-form solution for wedge cutting force through thin metal sheets. *International Journal of Mechanical Sciences*, vol. 35, no. 3-4, pp. 209–229.

Williams, J.; Rink, M. (2007): The standardisation of the ewf test. *Engineering Fracture Mechanics*, vol. 74, no. 7, pp. 1009–1017.

Zavattieri, P. D. (2006): Modeling of crack propagation in thin-walled structures using a cohesive model for shell elements. *Journal of Applied Mechanics*, vol. 73, no. 6, pp. 948–958.

Zheng, Z. M.; Wierzbicki, T. (1996): A theoretical study of steady-state wedge cutting through metal plates. *International Journal of Fracture*, vol. 78, no. 1, pp. 45–66.

Zienkiewicz, O. C.; Zhu, J. Z. (1992): The superconvergent patch recovery and a posteriori error estimates. part 1: The recovery technique. *International Journal for Numerical Methods in Engineering*, vol. 33, no. 7, pp. 1331–1364.